methanol, and then dried under reduced pressure at 40 °C to yield 0.270 g of the light yellow-powdered **8**. ^{1}H NMR (600 MHz, DMSO-d_6-D_2O): δ 4.46–4.28 (br, -OC*H*(CH-)O-), δ 4.28–4.11 (br, -C(=O)C*H*-(OH)-), δ 4.11–3.95 (br, -C(=O)CH(OH)C*H*(OH)-), δ 3.90–3.28 (br, -C*H*(O-)C*H*(OH)C*H*$_2$OH, -C*H*(OH)-C*H*(OH)C*H*(OH)C*H*(O-)C*H*$_2$OH, overlapped with HOD signal), δ 3.28–2.96 (br, -C(=O)NHC*H*$_2$-), δ 2.96–2.70 (br, Cl•N*H*$_3$C*H*$_2$-), δ 2.20–2.01 (br, -C(=O)-C*H*$_2$-), δ 1.80–1.32 (br, -NCH$_2$C*H*$_2$CH$_2$Si-, -C(=O)-CH$_2$C*H*$_2$-), δ 1.28–1.13 (br, -CC*H*$_2$C-), δ 0.88–0.80 (br, -C*H*$_3$), δ 0.80–0.36 (br, -C*H*$_2$Si-).

Measurements

The IR spectra were recorded using a SHIMADZU FT/IR-8400 spectrometer. The ^{1}H NMR spectra (600 MHz) were recorded using a JEOL ECA600 spectrometer. The gel permeation chromatographic (GPC) analyses were performed by using a TOSOH CCPD with RI detector under the following conditions: Shodex GF-310 column with water as the eluent at a flow rate of 0.5 mL/min. The calibration curve was obtained using pullulan standards. The X-ray diffraction (XRD) measurements were conducted at a scanning speed of $2\theta = 0.2°$/min using a RINT 1200 (Rigaku Co., Ltd) diffractometer with Ni-filtered CuKα radiation ($\lambda = 0.15418$ nm). The scanning electron microscope (SEM) images were obtained using a Hitachi S-4100 electron microscope. The dynamic light scattering (DLS) measurement was performed on a Zetasizer 3000 (Malvern Instruments).

RESULTS AND DISCUSSION

*Reaction of **1** with **2***

As previously reported,[13] an introduction of **2** to **1** was performed by heating at 80 °C in the presence of triethylamine in DMF to prepare a rigid polysiloxane **3** having polyol moieties (Scheme 1). The obtained product **3** was soluble in water and DMSO, but insoluble in typical organic solvents such as methanol, acetone, chloroform, and *n*-hexane.

The IR spectrum of the product showed an absorption at 1150 cm^{-1} attributed to the Si-O bond of the polysiloxane, an absorption at 1080 cm^{-1} assigned to the C-O bond of the polyol moiety derived from **2**, and an absorption at 1650 cm^{-1} due to the C=O bond of the amido group. In addition, the ^{1}H NMR spectrum in D_2O of the product showed both signals due to **1** and **2**. Furthermore, a methylene signal (δ 3.41–3.10) neighboring the amido group was appeared at lower magnetic field compared with a signal (δ 3.06–2.91) neighboring the unreacted amino group. These spectroscopic results indicated that the product has the structure **3** connecting **1** with **2** by the covalent bonds. The functionality of **2** to **1** was calculated to be *ca.* 75% based on the integrated ratio of the methylene signal neighboring the amido group to the methylene signal neighboring the silicon atom.

The molecular weights of **3** and **1** were evaluated by GPC analyses with water as the eluent. The GPC peak of **3** was shifted to the range of higher molecular weight compared to that of **1**. The M_n values of **3** and **1** estimated using pullulan standards were 21,200 g/mol ($M_w/M_n = 1.33$) and 10,300 g/mol ($M_w/M_n = 1.41$), respectively.

The XRD profile of **3** showed three peaks with the *d*-value ratio of $1:1/\sqrt{3}:1/2$ assigned to the (100), (110), and (200) peaks, respectively, indicating that the product has a hexagonal phase. Additionally, the *d*-value of the (100) peak of **3** ($d = 1.76$ nm) was larger than that of **1** ($d = 1.41$ nm). This indicates that the hexagonal phase in solid state was maintained in spite of the increase in the *d*-value by introduction of **2** to **1**.

The above analytical data indicated that **2** efficiently reacted with the amino groups in **1**, giving rise to **3**. To introduce the sugar moieties such as galactose residues on the surface of **1** by means of this reaction manner, the following experiments were performed using lactobionolactone **4**.

*Synthesis of Hydrophilic Sugar-Polysiloxane Hybrid **5***

We investigated synthesis of galactose-functionalized polysiloxane hybrid **5** by the reaction of **4** with **1**. Procedures for synthesis of **5** were almost same as those of **3**. Since the reaction in DMF gave the insoluble product, however, we employed DMSO as the alternative solvent, which was favorable for this reaction system. When an introduction of **4** to **1** was performed by heating at 80 °C in the presence of triethylamine in DMSO (Scheme 2), the initial reaction system was heterogeneous, which gradually became homogeneous with progress of the reaction. After the product was isolated as the fraction insoluble in acetone, unreacted amino groups were converted to ammonium cations by addition of HCl methanol solution in order to increase solubility and stability of the product in water. The obtained product **5** was soluble in water and DMSO, but insoluble in typical organic solvents such as methanol, acetone, chloroform, and *n*-hexane.

The IR spectrum of the product showed absorptions at 1650 cm^{-1} attributed to the C=O bond of the amido group, indicating the introduction of **4** to **1**. The ^{1}H NMR spectrum in D_2O of the product in Figure 1 shows both signals derived from **1** and **4**. Furthermore, a methylene signal $\mathbf{H_c}$ neighboring the amido group appeared at lower magnetic field compared with a signal $\mathbf{H_{c'}}$ neighboring the unreacted amino group. These spectroscopic data support the structure **5** of

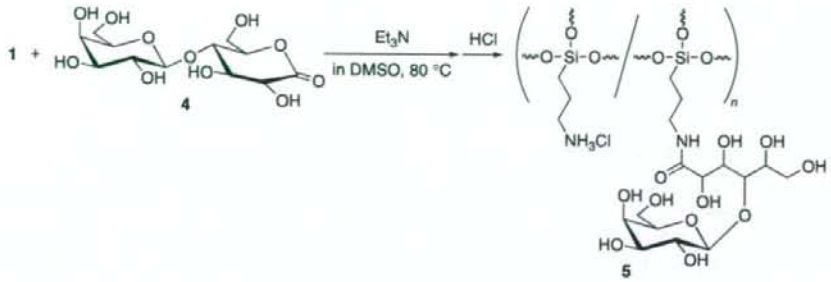

Scheme 2.

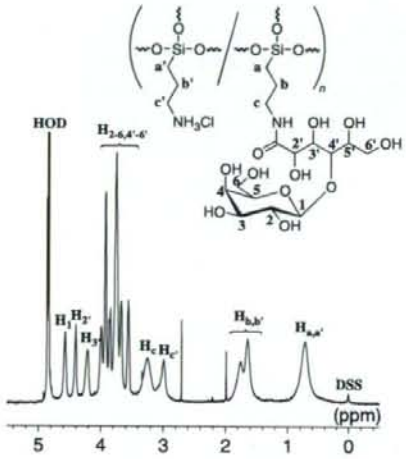

Figure 1. ^{1}H NMR spectrum of **5** in D_2O. Chemical shifts were referenced to sodium 2,2-dimethyl-2-silapentane-5-sulfonate (DSS) (δ 0.0 ppm).

the product. The functionality of **4** to **1** was calculated by the integrated ratio of the signal $\mathbf{H_1}$ to the signals $\mathbf{H_a}$ and $\mathbf{H_{a'}}$ in Figure 1 to be *ca.* 57%. Although the XRD profile of **3** showed three peaks for a typical hexagonal phase as described above, no diffraction peak was observed for **5**, indicating that a regular higher-ordered structure was not formed in the solid state. This would be because that the bulkiness of **4** affected the higher-ordered structure of **5**. However, **5** probably has the rigid structure in the solution due to the Si-O-Si network structure of the main-chain derived from trifunctional organoalkoxysilane. The molecular weight (M_n) of **5** estimated by GPC analysis with water as the eluent using pullulan standards was 44,700 g/mol ($M_w/M_n = 1.44$).

Synthesis of Amphiphilic Sugar-Polysiloxane Hybrid ***8***

To promote the formation of the nano aggregates of sugar-polysiloxane hybrid, we attempted synthesis of an amphiphilic hybrid **8** by introduction of the hydrophobic stearoyl groups in addition to the hydrophilic sugar groups on the surface of **5**. However, the reaction of **5** with stearoyl chloride **6** did not proceed to obtain **8**, probably due to bulkiness of sugar-residues existed on the surface of **5**. As an alternative reaction manner, an introduction of **6** to **1** was firstly carried out in the presence of triethylamine in water/DMF mixed solvent at room temperature to produce stearoyl-carrying polysiloxane **7** (Scheme 3). After addition of HCl aqueous solution to this reaction solution, the product was isolated as the fraction insoluble in acetone. The obtained product **7** was soluble in DMSO, but insoluble in water.

The IR spectrum of the product showed an absorption at 1640 cm^{-1} assigned to the C=O bond of the amido group. In addition, the ^{1}H NMR spectrum in DMSO-d_6 (including a small amount of D_2O) of the product in Figure 2 shows both signals derived from **1** and **6**. These spectroscopic results indicate the intro-

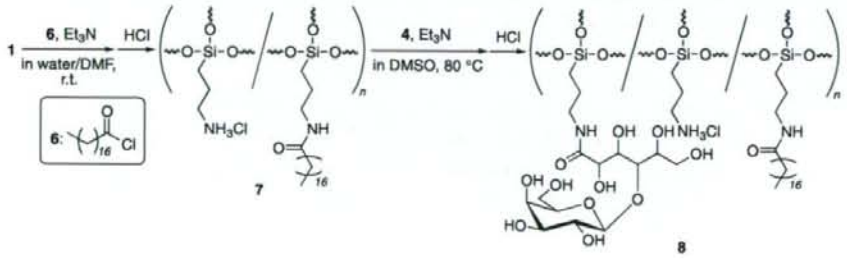

Scheme 3.

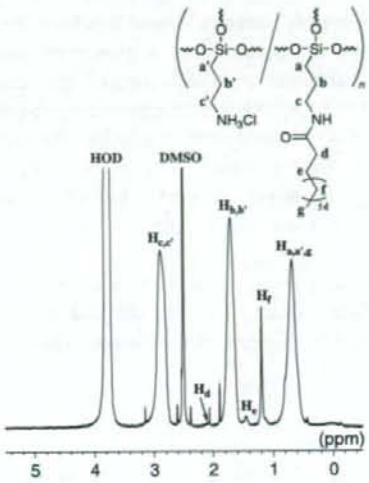

Figure 2. ^{1}H NMR spectrum of **7** in DMSO-d_6 (including a small amount of D_2O). Chemical shifts were referenced to DMSO (δ 2.5 ppm).

duction of **6** to **1**, leading to **7**. The functionality of **6** to **1** was calculated to be *ca.* 2% based on the integrated ratio of the signal $\mathbf{H_f}$ to the signal $\mathbf{H_b}$ and $\mathbf{H_{b'}}$. When the feed ratio of **6** to **1** was increased, the insoluble product was obtained.

As a second step, we carried out a reaction of **4** with **7** by heating at 80 °C in the presence of triethylamine in DMSO to obtain amphiphilic sugar-polysiloxane hybrid **8** (Scheme 3). The product was isolated as the fraction insoluble in acetone, followed by washing with acetone, HCl methanol solution, and methanol. The obtained product **8** was soluble in water and DMSO, but insoluble in typical organic solvents such as methanol, acetone, chloroform, and *n*-hexane.

The IR spectrum of the product showed an absorption at 1140 cm^{-1} attributed to the Si-O bond, an absorption at 1080 cm^{-1} assigned to the C-O bond of **4**, and an absorption at 1650 cm^{-1} due to the C=O bond of the amido group. Additionally, the ^{1}H NMR spectrum in DMSO-d_6 (including a small amount of D_2O) of the product in Figure 3a shows signals derived from **1**, **4**, and **6**. Furthermore, the methylene signals $\mathbf{H_a}$ and $\mathbf{H_b}$ of the product shift to higher field and the methylene signal $\mathbf{H_c}$ shifts to lower field compared with those of **7**. These shifts have also been observed in the synthesis of **3**,[13] and are attributed to progress of the amidation reaction of **7** with **4**. These spectroscopic results fully support the structure of the sugar- and stearoyl-functionalized polysiloxane **8**. The functionality of **4** to **1** was calculated by the integrated ratio of the signal $\mathbf{H_{f'}}$ to the signal $\mathbf{H_1}$ in Figure 3 to be *ca.* 48%, when the reaction was carried out under the conditions as described in experimental sec-

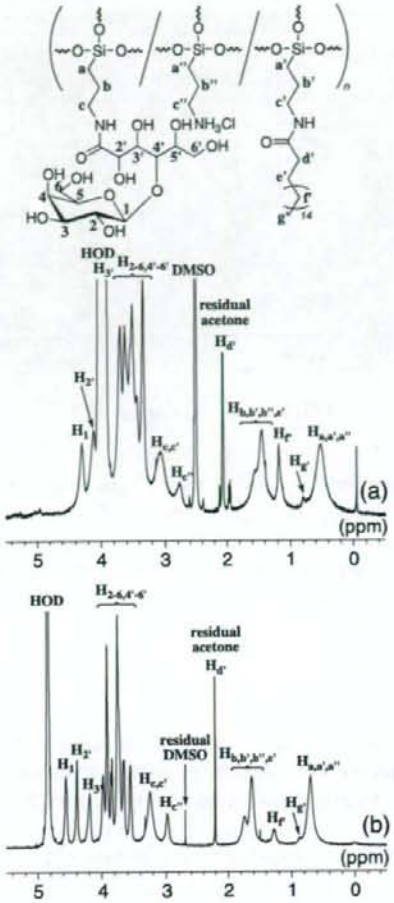

Figure 3. ^{1}H NMR spectrum of **8** (a) in DMSO-d_6 (including a small amount of D_2O) and (b) in D_2O. Chemical shifts were referenced to DMSO (δ 2.5 ppm) and DSS (δ 0.0 ppm), respectively.

tion. The functionalities were variable by changing the feed ratio of **4** to **7**.

Interestingly, intensity of a signal $\mathbf{H_{f'}}$ due to stearoyl group of **8** in D_2O decreases compared with that in DMSO-d_6 (Figure 3b). This observation indicates that the stearoyl groups existed in the inside of the intra and intermolecular aggregates of **8** in D_2O. To confirm the formation of nano aggregates of **8** in water, SEM image of **8** was taken. The SEM specimen was prepared by evaporating an aqueous solution of **8** on a spinning aluminium plate. The SEM image of the surface of **8** coated on the aluminum plate shows that nano aggregates were formed from **8** (Figure 4); nano aggregates having the particle diameters of *ca.* 50 nm are appearing at high frequency and larger particles that represent a diameter of *ca.* 500 nm are coexisting with smaller aggregates at much lower frequency (a few aggregates in a SEM image). The particle size

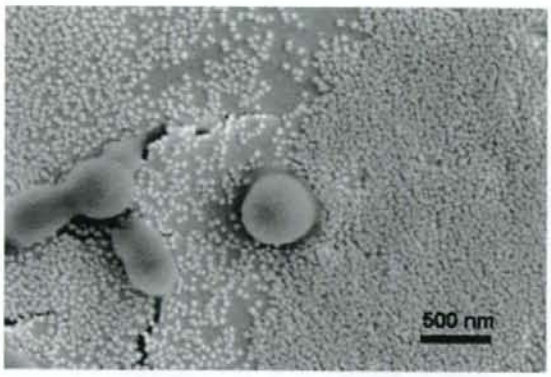

Figure 4. SEM image of **8**.

was also confirmed by dynamic light scattering (DLS) measurement. The mean diameter of the particle composed of **8** was 67.7 ± 4.5 nm (poly dispersity index: 0.273) in water. The aggregate size corresponds well to that was observed in the SEM image of the spin-coating sample of **8**.

CONCLUSIONS

The amino groups existed on the surface of the rigid polysiloxane (**1**) efficiently reacted with gluconolactone (**2**) to give the corresponding hybrid (**3**). This reaction manner was employed for preparation of the hydrophilic sugar-polysiloxane hybrid (**5**), which was achieved by the reaction of **1** with lactobionolactone (**4**). Furthermore, the amphiphilic sugar-polysiloxane hybrid (**8**) was also derived from **1** by the successive reactions with stearoyl chloride (**6**) and with **4**. The obtained hybrid materials **5** and **8** have galactose residues on their surfaces. Although hybrid **3** had the regular higher-ordered structure in the solid state, hydrophilic sugar-polysiloxane hybrid **5** did not form such a structure by the bulkiness of **4**. However, amphiphilic sugar-polysiloxane hybrid **8** formed the nano aggregates in water, which was confirmed by the ^{1}H NMR, SEM, and DLS analyses, expecting the multivalent effects of sugar-residues. The present materials are new class of sugar-inorganic hybrids, which have rigid polysiloxane main-chains.

Acknowledgment. The author (T.N.) thanks Dr. Tetsuji Yamaoka and Dr. Atsushi Mahara of National Cardiovascular Center for dynamic light scattering measurement.

REFERENCES

1. M. Okada, *Prog. Polym. Sci.*, **26**, 67 (2001).
2. K. Kobayashi, A. Tsuchida, T. Usui, and T. Akaike, *Macromolecules*, **30**, 2016 (1997).
3. X. L. Sun, K. M. Faucher, M. Houston, D. Grande, and E. L. Chaikof, *J. Am. Chem. Soc.*, **124**, 7258 (2002).
4. Q. Wang, J. S. Dordick, and R. J. Linhardt, *Chem. Mater.*, **14**, 3232 (2002).
5. A. B. Lowe, B. S. Sumerlin, and C. L. McCormick, *Polymer*, **44**, 6761 (2003).
6. L. Albertin, M. Stenzel, C. Barner-Kowollik, L. J. R. Foster, and T. P. Davis, *Macromolecules*, **37**, 7530 (2004).
7. G. Jonas and R. Stadler, *Acta. Polym.*, **45**, 14 (1994).
8. V. Braunmühl, G. Jonas, and R. Stadler, *Macromolecules*, **28**, 17 (1995).
9. V. Braunmühl and R. Stadler, *Polymer*, **39**, 1617 (1998).
10. K. Loos, G. Jonas, and R. Stadler, *Macromol. Chem. Phys.*, **202**, 3210 (2001).
11. Y. Kaneko, N. Iyi, K. Kurashima, T. Matsumoto, T. Fujita, and K. Kitamura, *Chem. Mater.*, **16**, 3417 (2004).
12. Y. Kaneko, N. Iyi, T. Matsumoto, and K. Kitamura, *Polymer*, **46**, 1828 (2005).
13. Y. Kaneko, J. Kadokawa, M. Setoguchi, and N. Iyi, *Polymer*, **46**, 8905 (2005).

JOURNAL OF BIOSCIENCE AND BIOENGINEERING
Vol. 103, No. 1, 98–100. 2007
DOI: 10.1263/jbb.103.98

High Inoculation Cell Density Could Accelerate the Differentiation of Human Bone Marrow Mesenchymal Stem Cells to Chondrocyte Cells

Mutsumi Takagi,[1]* Yousuke Umetsu,[1] Masashi Fujiwara,[1] and Shigeyuki Wakitani[2]

Division of Biotechnology and Macromolecular Chemistry, Graduate School of Engineering, Hokkaido University, N13W8, Kita-ku, Sapporo 060-8628, Japan[1] and Orthopedic Surgery, Osaka-City University School of Medicine, 1-4-3 Asahi-machi, Abeno-ku, Osaka, Osaka 545-8585, Japan[2]

Received 28 July 2006/Accepted 25 October 2006

The effects of the density of human mesenchymal stem cells (MSCs) on their differentioation to chondrocytes in a differentiation medium supplemented with dexamethasone, TGFβ3, and IGF-1 were investigated for the regenerative therapy of cartilage. The increase in the initial density of MSCs from 0.05×10^4 to 0.9×10^4 cells/cm^2 accelerated the increase in the expression level of aggrecan mRNA during the differentiation culture for 7 d. The conditioned medium harvested at 7 d from the differentiation culture with an initial MSC density of 0.3×10^4 cells/cm^2 accelerated the initial increase in the expression level for 3 d in the differentiation culture with an initial MSC density of 0.3×10^4 cells/cm^2, whereas the conditioned medium harvested at 7 d in the differentiation culture with an initial MSC density of 0.05×10^4 cells/cm^2 did not. The differentiation culture after 14 d with an initial MSC concentration of 0.3×10^4 cells/cm^2 showed an expression level 1.7-fold that in the case of the culture with an initial MSC concentration of 0.05×10^4 cells/cm^2. Thus, a high MSC inoculum density might be appropriate for the rapid differentiation of MSCs to chondrocytes.

[**Key words:** cell density, mesenchymal stem cell, differentiation, chondrocyte]

Combined addition of insulin-like growth factor (IGF)-1, transforming growth factor (TGF)-β3 and dexamethasone was effective for the differentiation of mesenchymal stem cells (MSCs) in adult bone marrow to chondrocyte cells (1). In general, cytokines produced by cultivated cells other than externally added cytokines to the culture, might affect cell differentiation. Thus, cell density should have some affect on cell differentiation because cytokine production rate depends on cell density. For example, an increase in initial stromal cell concentration from 0.4×10^5 to 2.7×10^5 cells/ml increased progenitor concentration during a three-dimensional coculture of murine bone marrow hematopoietic cells with murine bone marrow stromal cells (2). Moreover, initial cell density might be one of the easily adjustable operational variables.

Besides generally added cytokines such as TGF-β3 and IGF-1, cytokines secreted by MSCs have been considered to regulate the differentiation of MSCs to chondrocyte cells. However, it remains unclear how MSC density influences the differentiation of MSCs to chnodrocytes. Consequently, the effects of MSC density on MSC differentiation were investigated in this study.

MSCs were isolated from bone marrow aspirate obtained by routine iliac crest aspiration from human donors (age: 65–73) as previously reported (1). The content of $CD105^+$ $CD45^-$ cells among the cells analyzed by flowcytometer was approximately 90% (data not shown) (3).

The growth medium used was DMEM-LG (Gibco, NY, USA) supplemented with 10% FCS (Gibco), 2500 U/l penicillin, and 2.5 mg/l streptomycin.

The differentiation medium was DMEM-HG (Gibco) supplemented with 10% FCS, 2500 U/l penicillin, 2.5 mg/l streptomycin, 50 μg/ml L-ascorbic acid 2-phosphate (Wako Pure Chemicals, Osaka), 100 μg/ml sodium pyruvate (Wako), and 40 μg/ml proline (Wako). Growth factors, namely, 10 ng/ml TGF-β3 (Peprotech, Rocky Hill, NJ, USA), 39 ng/ml dexamethasone (ICN Biomedicals, Irvine, CA, USA), and 100 ng/ml insulin-like growth factor-I (IGF-I; Peprotech), were added.

The cells were cultured on a multiwell dish (9.6 cm^2; Sumitomo Bakelite, Tokyo) at densities of 0.05×10^4 to 0.9×10^4 cells/cm^2 employing the growth medium and allowed to attach for 1 d at 37°C in 5% CO_2. Then, the medium was replaced with the differentiation medium and differentiation culture was started. Cell density was determined by trypan blue dye exclusion after trypsinization.

The mRNA expression ratio of aggrecan, which is a typical extra cellular matrix produced by chondrocytes, to actin was determined by previously reported method emplying real-time RT-PCR (1) and employed as an index of differentiation of MSCs to chondrocytes.

* Corresponding author. e-mail: takagi-m@eng.hokudai.ac.jp
phone/fax: +81-(0)11-706-6567

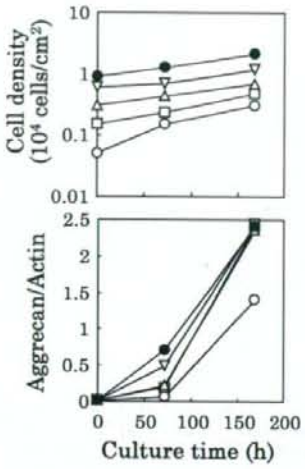

FIG. 1. Effect of initial cell density on expression level of aggrecan mRNA. Differentiation culture was performed for 7 d employing several inoculation cell densities of 0.05 (open circles), 0.15 (squares), 0.3 (triangles), 0.6 (inverted triangles), and 0.9 (closed circles)$\times 10^4$ cells/cm^2. The average of triplicate determinations is shown.

Differentiation culture was performed for 7 d employing several inoculation cell densities (0.05, 0.15, 0.3, 0.6, 0.9×10^4 cells/cm^2) and the expression level of aggrecan mRNA was determined (Fig. 1). The cells grew exponentially in all the cultures and there was almost no difference in specific cell growth rate between cultures that used different inoculum cell densities.

There was almost no expression of aggrecan mRNA at the initial time of differentiation culture (Fig. 1). Thereafter, the expression level increased monotonicaly until 168 h in all the cultures. At 72 h, the culture with the highest inoculation cell density showed the highest expression level. The aggrecan expression level in the culture with the lowest inoculum cell density was markedly lower than that of the other cultures at 168 h.

To confirm the presence of soluble factors produced by cells during the differentiation culture and the acceleration of the MSC differentiation, the conditioned media harvested on day 7 during the differentiation culture with the respective inoculum cell densities of 0.05 and 0.3×10^4 cells/cm^2 were employed for other differentiation cultures with the inoculum cell density of 0.3×10^4 cells/cm^2 for 3 d.

The aggrecan expression level in the culture using the conditioned medium from the culture with the initial cell density of 0.3×10^4 cells/cm^2 was markedly higher than that in the culture using the conditioned medium from the culture with the initial cell density of 0.05×10^4 cells/cm^2 (Fig. 2). It was also higher than the aggrecan expression level in the culture using the fresh medium.

It was revealed in previous experiments that a higher inoculum cell density results in a faster increase in the expression level of aggrecan mRNA during short-term culture such as 7 d. To confirm whether a higher inculum cell density leads to a higher expression level even in long-term culture, differentiation cultures with the inoculum cell densities

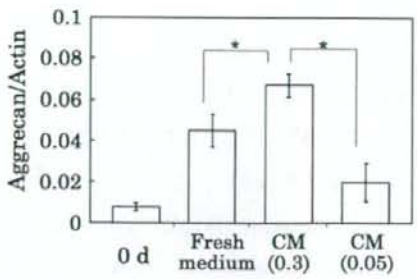

FIG. 2. Effect of conditioned medium on differentiation. Conditioned media were harvested at 7 d during the differentiation culture with inoculum cell densities of 0.05 and 0.3×10^4 cells/cm^2, respectively. Then, other differentiation cultures with an inoculum cell density of 0.3×10^4 cells/cm^2 for 3 d were performed employing fresh medium, and conditioned media from the cultures with inoculum cell densities of 0.05 (CM [0.05]) and 0.3×10^4 cells/cm^2 (CM [0.3]), respectively. Each bar indicates the standard deviation of triplicate culture. $P<0.05$.

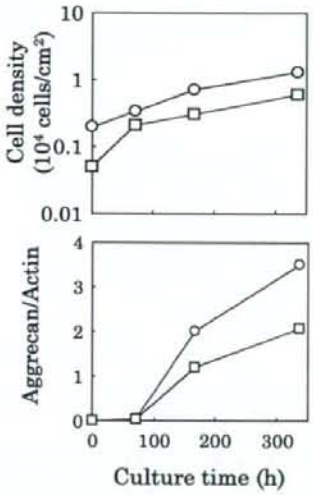

FIG. 3. Effect of inoculum cell density during long-term culture. The differentiation cultures with inoculum cell densities of 0.05 (squares) and 0.3×10^4 cells/cm^2 (circles) were performed for 14 d. Medium was changed weekly. The average of triplicate determinations is shown.

of 0.05 and 0.3×10^4 cells/cm^2 were performed for 14 d, with weekly medium changes.

The cells continued to grow until the end of culture (336 h) in both cultures with the inoculum cell densities of 0.05 and 0.3×10^4 cells/cm^2 (Fig. 3); there was no marked difference in growth rate between the cultures.

The aggrecan expression level at 169 h in the culture with the inoculum cell density of 0.3×10^4 cells/cm^2 was 1.69-fold that in the culture with the inoculum cell density of 0.05×10^4 cells/cm^2. Aggrecan expression level also continued to increase up to 336 h in both cultures. The expression level at 336 h in the culture with the higher inoculum cell density was also 1.69-fold that in the culture with the lower inoculum cell density.

The addition of TGF-β3 and IGF-1 initiated the differentiation of MSCs to chondrocytes, because almost no expression of aggrecan mRNA at 0 h of differentiation culture and a marked expression at 72 h were observed (Fig. 2). However, the expression level at 72 h differed between cultures with several inoculum cell densities in spite of the same concentrations of TGF-β3 and IGF-1 used. Thus, there might be factors other than TGF-β3 and IGF-1 affecting the expression of aggrecan mRNA in the culture. The other factors may not contain direct contact between cells, because the cultures did not reach confluence even at 168 h (data not shown). Moreover, the possible soluble factors may not affect cell growth rate, because the cell density employed in this study did not affect specific cell growth rate (Fig. 1).

The expression level of aggrecan mRNA reached 0.045 at 72 h with the use of fresh differentiation medium (Fig. 2), which was apparently lower than the expression level (0.26) at 72 h in the culture with the inoculum cell density of 0.3×10^4 cells/cm^2 obtained in an earlier experiment whose results are shown in Fig. 1. The reason for this difference may contain the difference in the condition of employed cells, because the expression level (0.022) at 0 h in the earlier experiment (Fig. 1) was higher than the expression level (0.008) in the later experiment (Fig. 2). However, the expression level in the culture using the conditioned medium from the culture with an initial cell density of 0.3×10^4 cells/cm^2 was markedly higher than those in both cultures using fresh medium and the conditioned medium from the culture with the initial cell density of 0.05×10^4 cells/cm^2 (Fig. 2). Consequently, the conditioned medium with the initial cell density of 0.3×10^4 cells/cm^2 might contain some soluble factors accelerating the increase in the expression level of aggrecan mRNA and the concentration of the possible soluble factors might be higher in the culture with the higher inoculum cell density. Not only the secretion of the soluble factors by cells but also the decomposition and inactivation of added factors such as TGF-β3 might occur during the culture. The later change may be dominant in the conditioned medium from the culture with the initial cell density of 0.05×10^4 cells/cm^2 and resulted in lower expression level compared with that with fresh medium. These may be the reason the expression level increased faster in the culture with the higher inoculum cell density (Fig. 1).

The concentration of soluble factors rather than cell density at each time during culture may affect the expression as mentioned above. Initial cell density might directly affect the time course of the concentration of the soluble factors. This may be the reason why the initial cell density apparently affected the increasing rate of expression level.

The concentration of cytokines produced in the cell culture was normally less than 1 ng/ml (2, 4). Thus, the possible soluble factors may be factors other than TGFβ3 and IGF1, whose concentrations in the fresh medium were 10 and 100 ng/ml, respectively.

The expression levels at 7 d (169 h) in the cultures with inoculum cell densities of 0.05 and 0.3×10^4 cells/cm^2 (1.19 and 2.02 in Fig. 3) were not so different from those at 7 d (168 h) in Fig. 1 (1.41 and 2.36), respectively. The fold increases in expression level due to the increase in the inoculum cell densities from 0.05 to 0.3×10^4 cells/cm^2 were 1.67 in Fig. 1 and 1.69 in Fig. 3, respectively. Thus, the effect of initial cell density on the increase in the expression level of aggrecan mRNA was quantitatively reproducible.

The fold increase in the expression level of aggrecan mRNA due to the increase in inoculum cell density from 0.05 to 0.3×10^4 cells/cm^2 was 1.69 at both 7 d (168 h) and 14 d (336 h) in Fig. 3. This shows that the effect of a higher inoculum cell density on the increase in the expression level was maintained for a long term such as 14 d. Besides, high inoculum cell density could reach to the same expression level (2.02 in Fig. 3) at 7 d as that (2.07 in Fig. 3) at 14 d in the culture with lower inoculum cell density. So, high inoculum cell density could decrease the length of culture period to the half that of lower inoculum cell density.

In conclusion, a higher inoculum MSC density accelerated the increase in the expression level of aggrecan mRNA in the differentiation medium supplemented with TGFβ3 and IGF-1. The fold increase caused by the higher inoculum cell density was quantitatively reproducible and maintained for at least 14 d. This effect may be due to some soluble factors produced by MSCs. Consequently, a higher inoculum MSC density might be appropriate for the differentiation of MSCs to chondrocyts for the regenerative therapy of cartilage.

REFERENCES

1. **Matsuda, C., Takagi, M., Hattori, T., Wakitani, S., and Yoshida, T.:** Differentiation of human bone marrow mesenchymal stem cells to chondrocytes for construction of three-dimensional cartilage tissue. Cytotechnology, **47**, 11–17 (2005).
2. **Takagi, M., Iemoto, N., and Yoshida, T.:** Effect of concentrations of murine stromal and hematopoietic cells on their three-dimensional coculture in nonwoven fabrics. J. Biosci. Bioeng., **94**, 365–367 (2002).
3. **Takagi, M., Nakamura, T., Matsuda, C., Hattori, T., Wakitani, S., and Yoshida, T.:** *In vitro* proliferation of human bone marrow mesenchymal stem cells employing donor serum and basic fibroblast growth factor. Cytotechnology, **43**, 89–96 (2003).
4. **Takagi, M., Horii, K., and Yoshida, T.:** Effect of pore diameter of porous membrane on progenitor content during a membrane—separated coculture of hematopoietic cells and stromal cell line. J. Artif. Organs, **6**, 130–137 (2003).

JOURNAL OF BIOSCIENCE AND BIOENGINEERING
Vol. 104, No. 6, 510–512. 2007
DOI: 10.1263/jbb.104.510

Effect of Static Pressure on Intracellular pH of Adhesive Chinese Hamster Ovary Cells

Masashi Fujiwara,[1] Satoru Koizumi,[1] and Mutsumi Takagi[1]*

Division of Biotechnology and Macromolecular Chemistry, Graduate School of Engineering, Hokkaido University, Kita 13, Nishi 8, Kita-ku, Sapporo 060-8628, Japan[1]

Received 26 June 2007/Accepted 3 September 2007

The effect of static pressure on the intracellular pH of the Chinese hamster ovary (CHO) cell line DR1000L4N was investigated. In cultivation of CHO cells at 0.9 MPa, two distinct populations were observed in the histogram of a flow cytometer, while single population was observed in cultivation at 0.1 MPa. The intracellular pH of the major population at 0.9 MPa was markedly lower than that of the single population at 0.1 MPa.

[**Key words:** static pressure, intracellular pH, Chinese hamster ovary cells]

Recently, the importance of mammalian cell culture for the production of pharmaceutical substances has been increasing owing to the efficient use of such culture for the production of not only interferons (1) and tissue plasminogen activator (tPA) (2) but also antibodies. Static pressure is one of the operational parameters that is effective in increasing the supply rate of dissolved oxygen in mammalian cell culture. Although the effects of pH, temperature, dissolved oxygen concentration and agitation rate on mammalian cell culture have been well documented, there are only few reports on the effect of static pressure on mammalian cells as discussed below.

We have reported that pressurized cultivation at 0.9 MPa increases the specific production rate of monoclonal antibodies by mouse hybridoma cells (3), tPA by human embryo lung (HEL) cells (4) and human-granulocyte-macrophage colony stimulating factor (hGM-CSF) by Chinese hamster ovary (CHO) cells (5), although there is almost no influence of such pressurization on specific cell growth rate. We also suggested that the transduction of a static pressure signal for the enhanced expression of hGM-CSF mRNA in CHO cells is via an extracellular-signal-related kinase (ERK) signaling cascade (6).

On the other hand, high hydrostatic pressure (40–60 MPa) evidently decreases the vacuolar pH of cells of the yeast *Saccharomyces cerevisiae* (7). The acidification of yeast vacuoles is explained by the influx of protons into vacuoles from an acidified cytoplasm under high hydrostatic pressure (8, 9). It is possible that a similar cytoplasm acidification occurs in CHO cells when high hydrostatic pressure is applied to the cells. The resulting low intracellular pH may positively affect the activity of cytoplasmic enzymes involved in hGM-CSF production. However, there are few reports on the intracellular pH in mammalian cells under high pressure, despite the fact that CHO cells are one of most useful mammalian cells for pharmaceutical production. In this study, the effect of static pressure on the intracellular pH of CHO cells was investigated.

CHO DR1000L4N cells producing hGM-CSF (10) were cultivated in Iscove's modified Dulbecco's medium (Sigma, St. Louis, MO, USA) supplemented with 10% dialyzed fetal bovine serum (Gibco, Grand Island, NY, USA), 0.1 mg/ml streptomycin (Sigma), 100 U/ml penicillin (Sigma) and 1 μM methotrexate (Sigma).

The cells were inoculated into 5 ml of the medium in T-flasks (25 cm^2; Sumilon, Tokyo) at a density of 1.5×10^4 cells/cm^2 and incubated in a CO_2 incubator for 24 h (37°C and 5% CO_2). Then, the flasks were placed in a pressurized incubator system consisting of four stainless-steel vessels (120 mm in length and 95 mm in inner diameter) sealed using flanges fitted with valves, a pressure gauge, and a PVA filter (5). The gas in the vessels were replaced with a gas mixture of 5% CO_2 and 95% air. Two vessels were further pressurized to 0.9 MPa using nitrogen gas. Culture temperature was maintained at 37°C using a water bath, and the pressurized vessels were not opened until the end of cultivation. The partial pressures of O_2 and CO_2 in the T-flasks in the vessels were respectively set at 0.021 and 0.005 MPa independent of static pressure to prevent changes in pH and dissolved oxygen concentration at different pressures. The pH of the medium in a centrifuge tube placed in the pressurized vessel was measured immediately after opening the vessels to confirm that there is no difference in CO_2 gas partial pressure between the pressurized vessels at 0.1 and 0.9 MPa (data not shown).

The cell concentration in the culture was determined by nuclei staining, in which adhering cells were incubated in a solution of 21 g/*l* citrate and 1 g/*l* crystal violet, and nuclei were counted under a microscope (11). The hGM-CSF concentration in the culture supernatant was determined using an enzyme-linked immunosorbent assay kit (Pierce Endogen, Rockford, IL, USA).

A fluorescent reagent, 2′,7′-bis(2-carboxyethyl)-5(6)-car-

* Corresponding author. e-mail: takagi-m@eng.hokudai.ac.jp
phone/fax: +81-(0)11-706-6567

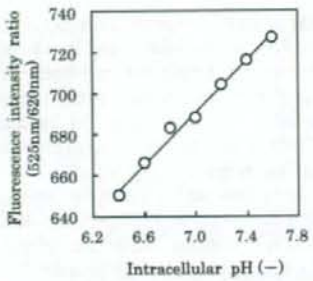

FIG. 1. Correlation between intracellular pH and fluorescence intensity ratio. CHO DR1000L4N cells were placed in high-[K^+] buffers (pHs 6.4, 6.6, 6.8, 7.0, 7.2, 7.4 and 7.6) for 5 min and incubated in EBSS buffer containing a fluorescent reagent, BCECF-AM, for 30 min. The fluorescence intensity of BCECF was measured at 525 nm and 620 nm using a flow cytometer. Internal pH was plotted against the mode of the ratio of the fluorescence intensity at 525 nm to that at 620 nm.

boxyfluorescein acetoxymethyl ester (BCECF-AM) (Sigma), was used for measuring the intracellular pH of CHO cells. The reagent permeates inside cells and is converted to the fluorescence dye BCECF through an intracellular esterase reaction, whose fluorescence intensity depends on intracellular pH. 5-(*N*-Ethyl-*N*-isopropyl) amiloride (EIPA, 100 μM) (Sigma) was added to cells in the late-logarithmic phase to maintain intracellular pH during BCECF-AM permeation. Then, the cells were harvested by trypsinization, washed once with EBSS buffer (sodium chloride, 140 mM; pottasium chloride, 5.4 mM; calcium chloride, 1.8 mM; magnesium sulfate, 0.8 mM; glucose, 5.0 mM, and HEPES 25 mM; pH 7.3±0.1), resuspended to a concentration of 1×10^7 cells/ml in EBSS buffer and incubated with 10 μM BCECF-AM for 30 min at room temperature. Fluorescence intensity was measured at 525 and 620 nm at an excitation of 488 nm using a flow cytometer (EPICS XL EXPO32 ADC; Beckman Coulter, Miami, FL, USA). CHO cells that were placed in high-[K^+] buffers (pHs 6.4, 6.6, 6.8, 7.0, 7.2, 7.4 and 7.6) containing 10 μM nigericin (Sigma) for 5 min, as mentioned above, were analyzed using a flow cytometer as controls and pH was plotted against the ratio of the intensity at 525 nm to that at 620 nm.

To precheck the accuracy of intracellular pH measurement, a calibration curve was plotted for CHO cells cultivated at 0.1 MPa. A good positive correlation was obtained between intracellular pH and fluorescence intensity ratio, as shown in Fig. 1.

After the adhesion of the CHO cells in the T-flask at 0.1 MPa for 24 h, the cells were cultured in the pressurized incubator at constant static pressures of 0.1 and 0.9 MPa. There was no marked difference between the cell densities on day 6 at 0.1 and 0.9 MPa (Table 1). Histograms of the

TABLE 1. Effect of static pressure on cell density of CHO cells at 143 h of cultivation

Pressure (MPa)	Cell density (10^5 cells/cm^2)
0.1	1.38±0.08
0.9	1.29±0.11

All results are expressed as means±SD (n=3).

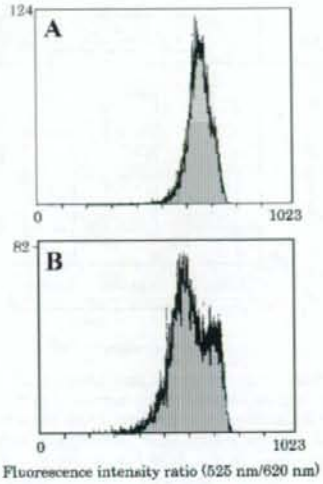

FIG. 2. Histogram of fluorescence intensity ratio. CHO DR1000L4N cells were cultured at constant pressures of 0.1 MPa (A) and 0.9 MPa (B) and incubated in EBSS buffer containing a fluorescent reagent, BCECF-AM, for 30 min. The fluorescence intensity of BCECF was measured at 525 nm and 620 nm using a flow cytometer. Total cell numbers in the histograms were 11391 (A) and 12948 (B), respectively.

fluorescence intensity ratio at 525 nm to that at 620 nm for the cells cultivated at 0.1 and 0.9 MPa are shown in Fig. 2. The histogram for the cells cultivated at 0.1 MPa showed a single peak whose ratio at 525 nm to that at 620 nm was approximately 650 (Fig. 2A). On the other hand, that for the cells cultivated at 0.9 MPa showed two distinct peaks. The ratio of mode for the larger peak (570) was lower than that for the cells cultivated at 0.1 MPa (650) (Fig. 2B). The smaller peak for the cells cultivated at 0.9 MPa had a higher ratio of mode (680) than that for the cells cultivated at 0.1 MPa (Fig. 2B).

The intracellular pHs at both 0.1 and 0.9 MPa of the CHO cells were calculated using the mode of the ratio in the histogram and calibration curve (Fig. 3). The intracellular pH for the larger peak of two populations in cultivation at 0.9 MPa (5.24±0.17) was markedly lower than that for the single peak at 0.1 MPa (6.60±0.76), and this difference (1.36) was considered significant at $P<0.05$ using a *t*-test. On the other hand, the intracellular pH for the smaller peak of the cells cultivated at 0.9 MPa was 6.77±0.09, which did not significantly differ from the intracellular pH of the cells cultivated at 0.1 MPa. Thus, it was found that increasing static pressure promotes cytoplasm acidification in major population of CHO cells.

Abe and Horikoshi have suggested that the following chemical reactions of CO_2, *i.e.*, hydration of carbon dioxide (Eq. 1) and ionization of carbonic acid (Eq. 2), contribute to cytoplasm acidification in yeast under high pressure (8, 9).

$$CO_2+H_2O \rightarrow H_2CO_3 \quad (1)$$

$$H_2CO_3 \rightarrow H^++HCO_3^- \quad (2)$$

$$CO_2+H_2O \rightarrow H^++HCO_3^- \quad (3)$$

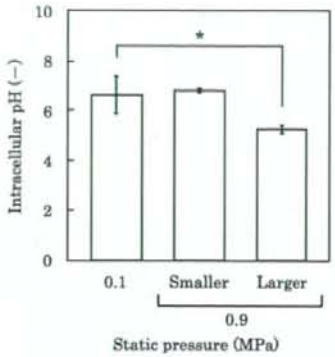

FIG. 3. Effect of static pressure on intracellular pH. CHO DR1000L4N cells were cultured at constant static pressures of 0.1 MPa and 0.9 MPa. The intracellular pH of CHO cells was determined from the mode of the ratio of the fluorescence intensities of BCECF measured by a flow cytometer. A single peak was observed at 0.1 MPa, and a larger peak and a smaller peak were observed at 0.9 MPa. The bar shows the SD of measurement (n=3) (asterisk: $P<0.05$).

The contribution of chemical reactions 1 and 2 to the reduction in the intracellular pH of CHO DR1000L4N cells was estimated as described below. The equilibrium equation in these two reactions can be represented by the equilibrium equation as follows (12):

$$\frac{\partial \ln k}{\partial P} = -\frac{\Delta V^{\neq}}{RT} \tag{4}$$

where P [atom] is the static pressure, k is the rate constant, $\Delta V^{\neq}$ is the volume of activation (=−26.0 ml/mol for Eq. 3), R is the gas constant (=8.31 J/K mol), and T is the absolute temperature (=310 K).

By substituting these values into Eq. 4, $\partial \ln k/\partial P$ can be calculated using

$$\frac{\partial \ln k}{\partial P} = -\frac{(-26.0)}{8.31\times 310} = 1.01\times 10^{-2} \tag{5}$$

When k_1 and k_2 are incorporated into Eq. 5 as rate constants at 0.1 MPa (P_1) and 0.9 MPa (P_2), respectively, Eq. 5 can be converted to

$$[\ln k]_{k_1}^{k_2} = 1.01\times 10^{-2}[P]_{P_1}^{P_2} \tag{6}$$

$$\frac{k_2}{k_1} = \exp(8.08\times 10^{-2}) = 1.08 \tag{7}$$

Equation 7 shows that the rate constant at 0.9 MPa (k_2) was 1.08 times larger than that at 0.1 MPa (k_1). Therefore, the difference between the pHs at 0.1 and 0.9 MPa (ΔpH) can be calculated based on the equilibrium of chemical reaction 2 as follows:

$$\Delta pH = \left(-\log k + \log\frac{[HCO_3^-]}{[H_2CO_3]}\right) - \left(-\log(1.08k) + \log\frac{[HCO_3^-]}{[H_2CO_3]}\right) = 0.033 \tag{8}$$

The calculated ΔpH (0.033) was considerably smaller than the experimentally observed ΔpH (1.36) in Fig. 3. This suggests that another mechanism, such as (i) proton generation from glycolytic intermediates and inorganic phosphates, and (ii) inactivation of the plasma membrane H^+-ATPase (8, 9), rather than the hydration and ionization of carbon dioxide, contribute to the decrease in the intracellular pH of pressurized CHO cells. Such other contributions should be investigated in the future.

There should be few report about the intracellular pH of mammalian cell culture under high pressure. In this study, we first quantitatively estimated the intracellular pH change in cultivation of CHO cells under high pressure by using a fluorescent reagent and a flow cytometer. It was found that the intracellular pH of major population of CHO DR1000L4N was obviously decreased when high pressure was applied to the cells.

REFERENCES

1. **Kawade, Y.:** Induction of antiviral resistance and interferon production in animal cell culture by exogenous RNA. Jpn. J. Med. Sci. Biol., **24**, 130–131 (1971).
2. **Dater, R. V., Cartwright, T., and Rosen, C. G.:** Process economics of animal cell and bacterial fermentations: a case study analysis of tissue plasminogen activator. Biotechnology, **11**, 349–357 (1993).
3. **Takagi, M., Ohara, K., and Yoshida, T.:** Effect of hydrostatic pressure on hybridoma cell metabolism. J. Ferment. Bioeng., **80**, 619–621 (1995).
4. **Takagi, M., Okumura, H., Okada, T., Kobayashi, N., Kiyota, T., and Ueda, K.:** An oxygen supply strategy for the large-scale production of tissue plasminogen activator by microcarrier cell culture. J. Ferment. Bioeng., **77**, 301–306 (1994).
5. **Gong, H., Takagi, M., Moriyama, T., Ohno, T., and Yoshida, T.:** Effect of static pressure on human granulocyte-macrophage stimulating factor (hGM-CSF) production by Chinese hamster ovary cells. J. Biosci. Bioeng., **94**, 271–274 (2002).
6. **Gong, M., Takagi, M., and Yoshida, T.:** Transduction of static pressure signal to expression of human granulocyte macrophage colony stimulating factor mRNA in Chinese hamster ovary cells. J. Biosci. Bioeng., **96**, 79–82 (2003).
7. **Abe, F. and Horikoshi, K.:** Hydrostatic pressure promotes the acidification of vacuoles in *Saccharomyces cerevisiae*. FEMS Microbiol. Lett., **130**, 307–312 (1995).
8. **Abe, F. and Horikoshi, K.:** Vacuolar acidification in *Saccharomyces cerevisiae* induced by elevated hydrostatic pressure is transient and is mediated by vacuolar H^+-ATPase. Extremophiles, **1**, 89–93 (1997).
9. **Abe, F. and Horikoshi, K.:** Analysis of intracellular pH in the yeast *Saccharomyces cerevisiae* under elevated hydrostatic pressure: a study in baro-(piezo-)physiology. Extremophiles, **2**, 223–228 (1998).
10. **Yoshikawa, T., Nakanishi, F., Ogura, Y., Oi, D., Omasa, T., Katakura, Y., Kishimoto, M., and Suga, K.:** Amplified gene location in chromosomal DNA affected recombinant protein production and stability of amplified genes. Biotechnol. Prog., **16**, 710–715 (2000).
11. **Sanford, K. K., Earle, W. R., Evans, V. J., Walts, H. K., and Shannon, J. E.:** The measurement of proliferation in tissue cultures by enumeration of cell nuclei. J. Natl. Cancer Inst., **11**, 773–795 (1951).
12. **Morild, E.:** The theory of pressure effect on enzymes. Adv. Protein Chem., **34**, 93–166 (1981).

Journal of Biomedical Optics 12(5), 054010 (September/October 2007)

Noninvasive measurement of three-dimensional morphology of adhered animal cells employing phase-shifting laser microscope

Mutsumi Takagi
Takayuki Kitabayashi
Syunsuke Ito
Masashi Fujiwara
Hokkaido University
Graduate School of Engineering
Division of Biotechnology and Macromolecular Chemistry
Sapporo 060-8628, Japan
E-mail: takagi-m@eng.hokudai.ac.jp

Akio Tokuda
FK Optical Laboratory
1-13-4 Nakano, Ni-iza
Saitama 352-0005, Japan

Abstract. Noninvasive measurement of 3-D morphology of adhered animal cells employing a phase-shifting laser microscope (PLM) is investigated, in which the phase shift for each pixel in the view field caused by cell height and the difference in refractive indices between the cells and the medium is determined. By employing saline with different refractive indices instead of a culture medium, the refractive index of the cells, which is necessary for the determination of cell height, is determined under PLM. The observed height of Chinese hamster ovary (CHO) cells cultivated under higher osmolarity is lower than that of the cells cultivated under physiological osmolarity, which is in agreement with previous data observed under an atomic force microscope (AFM). Maximum heights of human bone marrow mesenchymal stem cells and human umbilical cord vein endothelial cells measured under PLM and AFM agree well with each other. The maximum height of nonadherent spherical CHO cells observed under PLM is comparable to the cell diameter measured under a phase contrast inverted microscope. Laser irradiation, which is necessary for the observation under PLM, did not affect 3-D cell morphology. In conclusion, 3-D morphology of adhered animal cells can be noninvasively measured under PLM.
[DOI: 10.1117/1.2779350]

Keywords: morphology; noninvasive; three dimensional; laser microscope.

Paper 06215R received Aug. 8, 2006; revised manuscript received Mar. 19, 2007; accepted for publication May 15, 2007; published online Sep. 12, 2007.

1 Introduction

Animal cell cultivation is a very important technology for pharmaceutical production and cell processing for regenerative medicine. To optimize and control the quality of cells during cultivation, monitoring of cell quantity and quality can be carried out nondestructively and noninvasively, especially in cell processing for transplantation and regenerative medicine. Although light microscopic observation is useful for the noninvasive monitoring of adhered animal cells, this technique cannot facilitate 3-D morphological observation, but only 2-D morphological observation.

An atomic force microscope (AFM) can be used to observe the 3-D morphology of adhered animal cells. For example, the differences in 3-D morphology between Chinese hamster ovary (CHO) cells cultivated under various osmolarities were measured under AFM after fixation treatment of cells.[1] Because 3-D observation of adhered animal cells using AFM requires a long time and fixing treatment of cells, AFM observation is considered invasive for cells.

Recently, a novel phase-shifting laser microscope (PLM) was developed.[2] A biprism, located between the magnifying lens and the observation plane, was used as a beamsplitter. (Fig. 1) The biprism was laterally translated to introduce phase shifts required for quantitative phase measurement with a phase-shifting technique. Namely, the phase shift ($\Delta\Phi$) caused by the difference in refractive indices between the sample and the reference expressed in Eq. (1) can be determined using PLM.

$$\Delta\Phi = 2\pi d \times \frac{n_1 - n_0}{\lambda_0}, \tag{1}$$

where $\Delta\Phi$ is the phase shift (-); d is the thickness of the sample (nanometers); λ_0 is the wavelength of the laser (nm); and n_1 and n_0 are the refractive indices of the sample and reference (-), respectively. We believe that PLM may be applicable for measuring the thickness (d) of living adhered cells by substituting the refractive indices of cells and the medium to n_1 and n_0 in Eq. (1), respectively.

In this study, noninvasive 3-D observation of animal cells under PLM without fixing treatment was investigated.

Address all correspondence to Mutsumi Takagi, Graduate School of Engineering Hokkaido University N13, W8 - Sapporo, Hokkaido 060-8628 Japan; Tel: +81-11-706-6567; Fax: +81-11-706-6567; E-mail: takagi-m@eng.hokudai.ac.jp

1083-3668/2007/12(5)/054010/5/$25.00 © 2007 SPIE

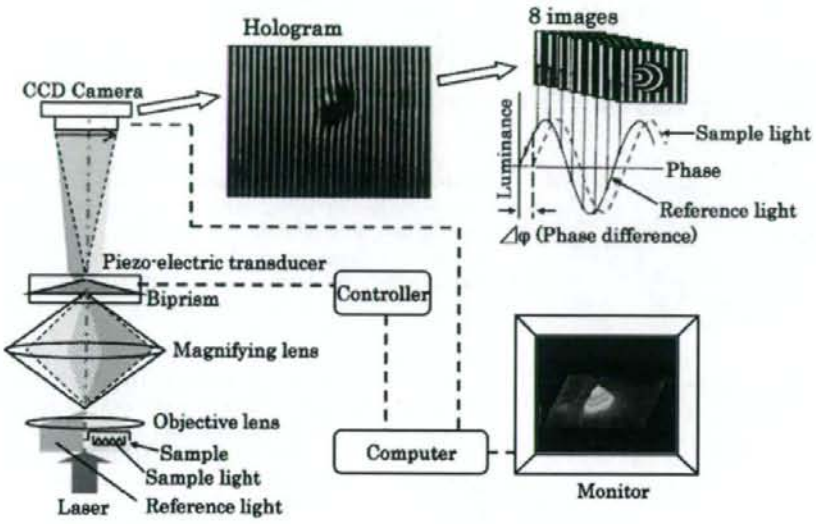

Fig. 1 Schematic diagram of phase-shifting laser microscope.

2 Materials and Methods

2.1 *Cells and Media*

Tissue plasminogen activator (tPA)-producing Chinese hamster ovary (CHO) 1-15500 cells (ATCC CRL-9606) were used. Ham's F-12K medium (Dainippon Seiyaku Company, Limited, Japan) supplemented with 10% newborn bovine serum (NBS, Gibco, New York), streptomycin (0.1 mg/L), and penicillin (100 u/L) was employed for cell growth. Medium osmolarity was adjusted to 300 and 400 mOsm/L by the addition of NaCl solution (100 g/L). Medium osmolarity was determined by measuring the depression of the freezing point using an osmometer (model OM-801, Vogel, Germany). CHO cells (6.7×10^4 cells) were inoculated into 2 ml of the medium in a dish (Falcon, 9.6 cm^2) and incubated for 4 d in a CO_2 incubator (37°C, 5% CO_2). Cell suspension was prepared by trypsinization of adhered cells on a dish.

Human bone marrow mesenchymal stem cells (MSCs) were isolated from bone marrow aspirate obtained by routine iliac crest aspiration from human donors (age 65 to 73) as previously reported.[3] The content of $CD105^+$ $CD45^-$ cells among the cells analyzed by a flowcytometer was approximately 90% (data not shown).[4] MSCs were cultured at densities of 0.15×10^4 cells/cm^2 employing DMEM-LG (Gibco, New York) supplemented with 10% Fetal Calf Serum (FCS) (Gibco), 2500 U/l penicillin, and 2.5 mg/l streptomycin.

Human umbilical cord vein endothelial cells (HUVEC) were purchased from Cambrex Bio Science Walkersville, Incorporated (Maryland) and cultured at densities of 0.2×10^4 cells/cm^2 employing DMEM (Gibco, Japan) supplemented with 10% inactivated fetal bovine serum (Gibco), 1 aliquot (of the same concentration as that in MEM) of MEM nonessential amino acids (Gibco), 2-mM glutamine, 5000 U/L penicillin, and 5 mg/L streptomycin (Sigma, Missouri).

2.2 *Cell Morphology Analysis under Phase-Shifting Laser Microscope*

The adhered cells on the bottom surface of the culture dish were observed under PLM. Two neighboring fields of view with cells and without cells were selected as sample and reference fields, respectively, and phase shift ($\Delta\Phi$) was determined for all pixels in the sample field under PLM. By substituting the wavelength of the laser (λ_0=632.8 nm), the refractive indices of the cells determined by the method mentioned later (n_1=1.39, 1.375, and 1.375 for CHO, MSC, and HUVEC, respectively) and the medium (n_0=1.34), and the measured phase shift ($\Delta\Phi$) to Eq. (2), the height of the cells (d nm) was calculated for all pixels in the sample field, and a 3-D view of the sample field was made.

$$d = \frac{\Delta\Phi}{2\pi} \times \frac{\lambda_0}{n_1 - n_0} \tag{2}$$

2.3 *Determination of Refractive Index of Cells*

The culture medium was replaced with saline containing different concentrations of bovine serum albumin (380 to 480 g/L), in which osmolarity was adjusted to the original medium osmolarity, and cells were observed under PLM. The refractive index of the saline, with which cell images disapperared under PLM, was considered as the refractive index of the cells. The refractive indices of the medium and saline were determined using a refract meter (DR-A1, Atago Company, Tokyo, Japan).

2.4 *Cell Observation under Atomic Force Microscope*

Cells were fixed with glutaraldehyde (4%), dried, and analyzed using an atomic force microscope (AFM)(NanoScope

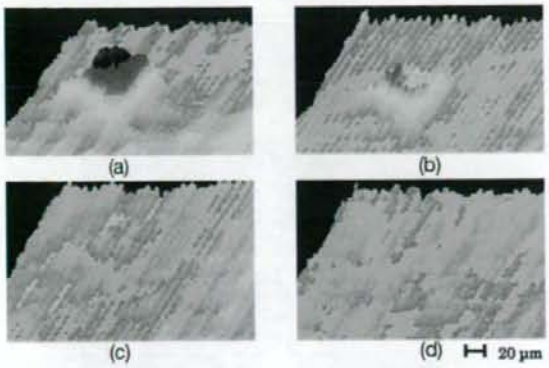

Fig. 2 Determination of refractive index of adhered CHO cells. CHO cells adhered to a culture dish containing saline with known refractive indices (a) 1.33, (b) 1.34, (c) 1.38, and (d) 1.39 were observed under PLM. The color bar is analogous to that in Fig. 3.

IIIa, Veeco). Namely, the height was scanned for all parts of each cell, and the closed area showing positive height was defined as the cell adhesive area.[5]

3 Results and Discussion

3.1 *Determination of Refractive Index of Adhered Chinese Hamster Ovary Cells*

After the CHO cells in the culture medium were observed under PLM, the culture medium was replaced with saline containing albumin while the culture dish was fixed on the stage of PLM. Cell image was distinct with the saline, having refractive indices of 1.33 and 1.34 (Fig. 2). Cell image was indistinct for the saline refractive index of 1.38 and was not observed for the saline refractive index of 1.39. Consequently, the refractive index of the observed CHO cells was determined to be 1.39.

The refractive index of the cell membrane (1.5) is higher than that of the cytoplasm (1.35),[6] and the thickness of the cell membrane is approximately 7.5 nm.[7] Because the adopted refractive index for CHO cells in this study (1.39) was between 1.35 and 1.5, it may be the sum of the refractive indices of the cell membrane and cytoplasm. However, the digit of significant figures must increase to increase the accuracy of the cell height measurement under PLM in the future, because the difference in refractive index between the cells and the medium was small (e.g., 0.05).

3.2 *Effect of Osmolarity on Three-Dimensional Cell Morphology Observed under Phase-Shifting Laser Microscope*

CHO cells cultivated for 4 *d* under different osmolarities of 300 and 400 mOsm/L were observed under PLM [Figs. 3(a) and 3(b)]. The 2-D morphology of the CHO cells cultivated under 400 mOsm/L was elongated, while that of the CHO cells cultivated under 300 mOsm/L was globular. This difference in the 2-D cell morphology between the CHO cells cultivated under different osmolarities is in agreement with previous observations not only under AFM, but also under a conventional light-inverted microscope.[1]

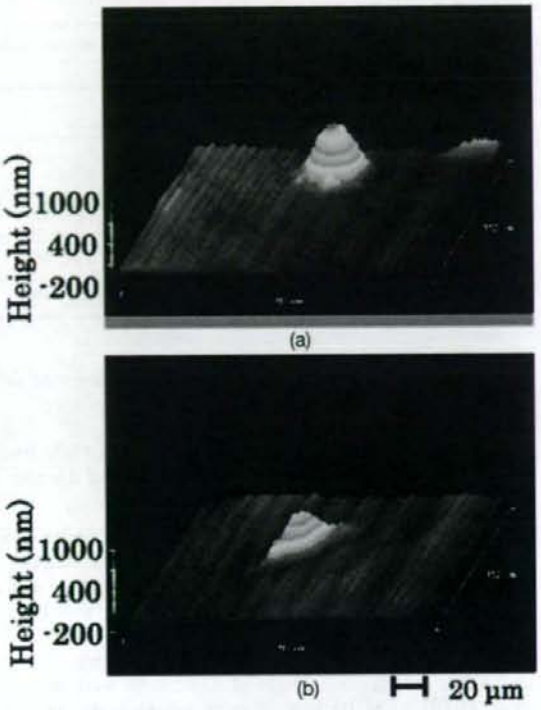

Fig. 3 Observation of CHO cells cultivated under different osmolarities under PLM. 3-D views of CHO cells cultivated under (a) 300 and (b) 400 mOsm/L.

The height of the CHO cells cultivated under 400 mOsm/L [Fig. 3(b)] was lower than that of the CHO cells cultivated under 300 mOsm/L [Fig. 3(a)]. The comparison of the average value for each ten cells showed that the cell maximum height under 400 mOsm/L was apparently lower than that under 300 mOsm/L (Fig. 4). This dependency of cell height on osmolarity is in agreement with a previous report observed under AFM.[1] Moreover, there was no marked difference between the measured values under PLM and AFM

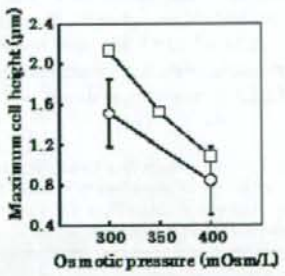

Fig. 4 Effect of osmolarities on maximum cell height. The maximum height of each cell (n=10, mean±SD) observed under PLM (circle) was plotted against osmolarity together with that of each cell observed under AFM (square).

Table 1 Cell maximum height measurement under PLM and AFM. The maximum height of each cell (n=10, mean±SD) observed under PLM and AFM are shown.

Cell species	Cell maximum height (μm)	
	PLM	AFM
CHO	2.00±0.92	2.06±0.63
MSC	1.52±0.79	1.73±0.46
HUVEC	1.09±0.92	1.20±0.30

(Fig. 4). These results strongly suggest the accuracy of cell height measurement using PLM.

3.3 *Comparison of Maximum Cell Heights Measured by Phase-Shifting Laser Microscope and Atomic Force Microscope for Various Cell Species*

To confirm the accuracy of measured cell height under PLM and the applicability of PLM to various kinds of animal cells, adhesive CHO, MSC, and HUVEC cells were observed under PLM without fixation and AFM with fixation and drying (Table 1). Average cell height of CHO cells was higher than those of MSC and HUVEC in both measurements of PLM and AFM. Average cell height of MSC cells were between those of CHO and HUVEC in both measurements of PLM and AFM. Average cell heights measured by PLM were near to those measured by AFM in all cell kinds, while the standard deviations for PLM measurement were a little larger than those for AFM measurement. These data can show that the accuracy of cell height measurement by PLM and PLM measurement should be applicable to various cell species.

3.4 *Comparison of Maximum Height Measured by Phase-Shifting Microscope and Two-Dimensional Diameter for Nonadherent Spherical Chinese Hamster Ovary Cells*

To confirm the accuracy of maximum cell height measure by PLM, maximum cell height of nonadherent spherical CHO cells measured by PLM was compared with their horizontal diameter measured by PLM or conventional inverted microscope. Nonadherent CHO cells were prepared by tripsinization of adherent cells and measured in medium (Table 2). There was no marked difference in the horizontal diameter of cells between PLM (7.33±1.49) and inverted microscope (8.78±1.20) measurements. Cell maximum height measured by PLM (5.68±2.53) was comparable to cell diameters. Cell

Table 2 Observation of nonadherent CHO cells under PLM. Diameter and maximum height of nonadherent spherical CHO cells were measured by the observation under PLM and inverted phase contrast microscope. Mean±SD (n=10) are shown.

Cell maximum height (μm)	Cell diameter (μm)	
PLM	PLM	Inverted microscope
5.68±2.53	7.33±1.49	8.78±1.20

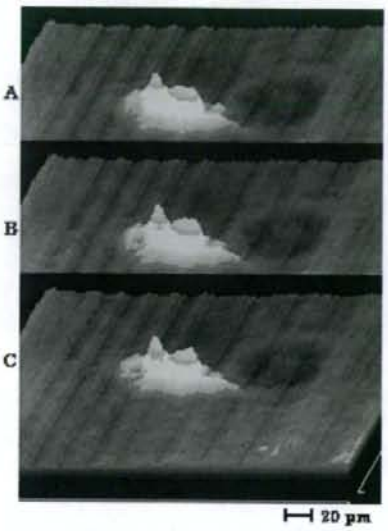

Fig. 5 Influence of laser irradiation on 3-D cell morphology of CHO cells. The time lengths of laser irradiation for CHO cells before observation under PLM were (a) 0, (b) 5, and (c) 10 min, respectively. The color bar is analogous to that in Fig. 3 (color online only).

maximum height (5.68±2.53) measured by PLM was smaller than the horizontal diameter (7.33±1.49) measured by PLM. This shows that cell height was a little smaller than the horizontal diameter due to the gravity force. These data support the accuracy of cell height measurement by PLM.

3.5 *Influence of Laser Irradiation on Cell Morphology*

To confirm the influence of laser irradiation required for PLM observation on cell morphology, a dish containing adhered CHO cells was set on the stage of a PLM and received continuous irradiation of a laser for 10 min, during which a 3-D cell morphology was observed at 0, 5, and 10 min, respectively (Fig. 5). There was no marked change in the 3-D cell morphology of the CHO cells during the laser irradiation for 10 min.

The laser irradiation dose required for PLM observation was less than 0.1 mW, and may not influence 3-D cell morphology, because an observation of one sample under PLM took only 30 s.

The spatial resolution in cell height observed under PLM should be approximately 10 to 2 nm, because the resolution in phase shift is 10 to 5 rad and the difference in refractive index between cell and medium is 0.04. This resolution under PLM might be comparable with or better than that observed under AFM. Cells adhered on the bottom of a conventional culture dish can be observed under PLM *in situ* together with culture medium, while cells need to attach onto some special board and liquid culture medium should be removed for observation under AFM. So, PLM observation might be noninvasive compared to AFM observation. Observation of cells under PLM takes only a few minutes and needs no special training, because 3-D morphology can be observed for voluntary cells selected under a normal light inverted microscope. Moreover,

there is almost no restriction for cell height observed under PLM, while cell height observed under AFM is limited by the size of the lever (e.g., 5 μm). Consequently, the observation of 3-D cell morphology under PLM might be more attractive for academic and pharmaceutical research compared to AFM observation.

4 Conclusion

These data show that PLM can quantitatively measure the 3-D morphology of adhesive animal cells noninvasively.

References

1. M. Takagi, H. Hayashi, and T. Yoshida, "The effect of osmolarity on metabolism and morphology in adhesion and suspension Chinese hamster ovary cells producing tissue plasminogen activator," *Cytotechnology* **32**, 171–179 (2000).
2. J. Endo, J. Chen, D. Kobayashi, Y. Wada, and H. Fujita, "Transmission laser microscope using the phase-shifting technique and its application to measurement of optical waveguides," *Appl. Opt.* **41**(7), 1308–1314 (2002).
3. C. Matsuda, M. Takagi, T. Hattori, S. Wakitani, and T. Yoshida, "Differentiation of human bone marrow mesenchymal stem cells to chondrocytes for construction of three-dimensional cartilage tissue," *Cytotechnology* **47**, 11–17 (2005).
4. M. Takagi, T. Nakamura, C. Matsuda, T. Hattori, S. Wakitani, and T. Yoshida, "In vitro proliferation of human bone marrow mesenchymal stem cells employing donor serum and basic fibroblast growth factor," *Cytotechnology* **43**(1-3), 89–96 (2003).
5. H. J. Butt, E. K. Wolff, S. A. Gould, N. B. Dixon, C. M. Peterson, and P. K. Hansma, "Imaging cells with the atomic force microscope," *J. Struct. Biol.* **105**, 54–61 (1990).
6. J. Sonke and A. W. Edith, "The physical basis of transparency in biological tissue: Ultrastructure and minimization of light scattering," *J. Theor. Biol.* **199**, 181–198 (1999).
7. A. M. Richard, "Light scattering from biological cells: dependence of backscatter radiation on membrane thickness and refractive index," *Appl. Opt.* **18**(5), 585–588 (1979).

Available online at www.sciencedirect.com
ScienceDirect
Behavioural Brain Research 179 (2007) 90–98
BEHAVIOURAL BRAIN RESEARCH
www.elsevier.com/locate/bbr

Research report

Environmental change during postnatal development alters behaviour, cognitions and neurogenesis of mice

Hiroyuki Iso [a,*], Shigero Simoda [a], Tomohiro Matsuyama [b]

[a] *Department of Behaviour Science, Hyogo College of Medicine, 1-1 Mukogawa-cho, Nishinomiya, Hyogo 663-8501, Japan*
[b] *Institute for Advanced Medical Sciences, Hyogo College of Medicine, 1-1 Mukogawa-cho, Nishinomiya, Hyogo 663-8501, Japan*

Received 22 March 2006; received in revised form 4 January 2007; accepted 23 January 2007
Available online 3 February 2007

Abstract

Four groups of male C57BL/6 mice were reared differing combinations of the two environments from 3 to 11 weeks after birth. At 12 and 13 weeks they were assessed by measures of behaviour and learning: open-field activity, auditory startle reflex and prepulse inhibition, water maze learning, and passive avoidance. Another four groups of mice reared under these varying conditions were examined for generation of neurons in hippocampus and cerebral cortex using bromodeoxyuridine (BrdU) at 12 weeks. Enriched (EE) and impoverished (PP) groups were housed in their respective environment for 8 weeks, enriched–impoverished (EP) and impoverished–enriched (PE) mice respectively were reared for 6 weeks in the first-mentioned environment and then for 2 weeks in the second. PP and EP mice showed hyperactivity, greater startle amplitude and significantly slower learning in a water maze than EE or PE animals, and also showed a memory deficit in a probe test, avoidance performance did not differ. Neural generation was greater in the EE and PE than PP and EP groups, especially in the hippocampus. These results suggest that environmental change critically affects behavioural and anatomic brain development, even if brief. In these mice, the effect of unfavourable early experience could be reversed by a later short of favourable experience.

Keywords: Enrichment; Impoverishment; Environmental change; Behaviour; Neuronal generation; Mice

1. Introduction

Research concerning environmental enrichment has been carried out since 1960s. Earlier studies reported that rats reared for a few months following weaning in a group in a large cage with a running wheel, toys and a hiding had greater brain weights and showed more acetylcholinesterase activity than animals reared alone in a small cage for the same period even though both environments had food and water continuously available [38,40]. Some authors suspected that an increase in glial cells might have contributed to these differences [2]. Later, rats spending earlier life in an enriched environment had been reported to show lower activity in open field test than rats spending the same period in an impoverished setting with little stimulation [17]. Still other reports indicated that even brief exposure to the enriched environment affected development of brain and behaviour in rats [11,12]. In recent studies involving rats, an enriched developmental environment was reported to increase neurotrophic factor gene expression [29], brain-derived neurotrophic factor protein [30], numbers of hippocampal neurons [20,21,48,49], and dendritic growth, in association with improvements in behaviour and cognition [22]. Recovery from transient global ischemia was reported clinically to be promoted by environment enrichment [15]. Environmental enrichment also was reported to promote normal emotional behaviour and even immune function under stress [5]. Even "knockout" mice with a genetically mediated hippocampal deficit causing behavioural and memory deficiencies were reported to improve their ability to learn after a period of exposure to an enriched environment [8,35]. Thus, a benefit from environmental enrichment during development of animals concerning behaviour, neurophysiology, neuroanatomy, and even immunity has been reported and even applied to humans [16,36,37].

On the other hand, some authors point out that an enriched environment is the natural situation in animal neurologic development, while environmental impoverishment is an artificial

Abbreviations: BrdU, 5-bromo-2′-deoxyuridine; PSA-NCAM, polysialylated neuronal cell adhesion molecule

* Corresponding author. Tel.: +81 798456378; fax: +81 798456378.
E-mail address: iso@hyo-med.ac.jp (H. Iso).

0166-4328/$ – see front matter © 2007 Elsevier B.V. All rights reserved.
doi:10.1016/j.bbr.2007.01.025

condition inducing neurologic maldevelopment [27,41]. Indeed, rats housed singly can show abnormal behaviours, such as attention deficiency, hyperactivity, exaggerated emotional behaviour, and stereotypy [6,51], accompanied by evidence of neurochemical change [24,31,32]. Lack of manipulation during infancy also was reported to impair learning and memory in the adult rat [34]. Socially isolated animals even have been studied as a model of human psychotic illness [6]. Some animal studies also have examined whether or not resocialization could reverse effects of social isolation. Hyperactivity and hypoanalgesia [14] as well as deficient in water-maze learning [50] in impoverished rats has been demonstrated to be reversible upon resocialization. However, other studies where impoverishment started at weaning period failed to show this effect [9,13], suggest that the developing brain is susceptible to permanent changes at an earlier age. Wright et al. [51] reported that rats reared in an impoverished environment for 30 days after weaning, could not reverse their profile of anxious behaviour in X-maze performance after resocialization for 30 days. The performance of rats experiencing the reverse condition (a change from enriched to impoverished environments) did not differ from that in the enrichment group. Thus, reversal of environmental conditions 30 days after weaning did not affect the animals' emotional profiles. Katz and Davies [19] tested the effects of environmental manipulation during developing period on the neuroanatomy of the rats using a factorial design. Two groups of animals were reared in the enriched or impoverished environment for 2 months. Another two groups of rats were housed enriched or impoverished environment for 1 month, then the housing condition was changed to impoverished or enriched in the next month, respectively. The neuroanatomical outcomes of the enriched and impoverished groups supported to earlier reports by Rosenzweig et al. [38,40] that enriched rats had heavier brain weight, longer cerebral length and greater cortical thickness than impoverished rats. The results of the two exchange groups showed that animals which experienced enriched housing whichever during early or later 1 month developed their brain as same as the enriched group. Thus, enrichment was beneficial for brain development, and development of the brain was not modified by impoverishment, once rats had experienced enrichment [19].

The finding of neurogenesis in the adult rat [43,44] involves methods for discriminating newly generated neurons from established cell masses in the various areas of the brain. Much evidence has accumulated about effects of environment on brain development [2,21–23,29,30,38]. Additionally, experience with running was reported to enhance neurogenesis and promoted long-term potentiation (LTP) and learning in mice [47,48]. Yet, little has been known about effects of environmental manipulation during development on generation of neurons in adult rodents [20,21,48,49].

Whether enrichment or impoverishment is a more important environmental influence on neural development, neuronal plasticity suggests that exposure of impoverished animals to an enriched environment will enhance behavioural performance, while the reverse sequence will impair performance even if it is a short duration [11,12]. The objects of the present experiment are to test whether the environmental manipulations, from enrichment to impoverishment, or impoverishment to enrichment affect to the behavioural and neuronal development in mice [19], because we have experienced behavioural and neuroanatomical experiments in mice [25,52,53,1,45] and mice were drawn attention as models of human behavioural and psychiatric diseases rather than rats due to the developing evidences by gene engineering [7].

2. Materials and methods

All procedures were performed in accordance with National Cardiovascular Center Animal Care and Use Protocol. Quantitative measurements including behavioural tests and microscopic assessments were performed by investigators without knowing identity of the animal or section under study.

2.1. Experiment 1: behaviour

The effect of environmental manipulations on activity, reflexes, attention and cognition, spatial learning and of memory of fear were examined.

2.1.1. Subjects

Forty-four male C57BL/6 mice, purchased from Nihon SLC (Shizuoka Japan) of age at 3 weeks were reared under four different housing conditions for 8 weeks. Tap water and food (MF chow, Oriental, Tokyo Japan) were continuously available. In the enriched (EE) group, mice were housed for 8 weeks four animals to a plastic cage (60 cm × 80 cm × 30 cm) containing plastic tubes as toys, a hiding place, and a running wheel. Mice in the impoverished (PP) group were housed for 8 weeks singly in a small plastic cage (20 cm × 30 cm × 20 cm) with no play materials. Enriched–impoverished (EP) mice first were housed like EE mice for 6 weeks and then like PP mice for 2 weeks. Impoverished–enriched (PE) mice were housed like PP mice for 6 weeks and then like EE mice for 2 weeks. Mice were handled once weekly for less than 1 min to weigh them and place them in clean cages. The two connected rooms where mice were housed and tested were air conditioned to maintain temperatures between 20 and 21 °C. Room lights were on from 7 a.m. to 7 p.m.

2.2. Apparatus and experimental protocol

Behavioural tests (one to four below) were conducted in order of description (and of increasing complexity) to avoid order effects [26]. The basic experimental settings of the open-field test, Morris water maze learning and passive avoidance task were reported previously [25,52]. All the behavioural tests were conducted during light period (10:00–16:00 h), and the group order of animals applied to each test was random. Mixed-type analyses of variance (ANOVA) were used for data analysis. Differences between groups were tested further with a post hoc test (Bonferroni/Dunn, with $p < .05$ defining significance).

2.2.1. Open-field test

Animals were allowed to move freely in a square acrylic box (30 cm × 30 cm) for 20 min. Ten minutes light period was followed by 10-min dark period. On X and Y sides of the open-field, two infrared beams were positioned 2 cm above the box floor at a 10-cm distance. A flip-flop circuit was set up between the two beams. The total number of beam crossings was counted as locomotive behaviour of the animal. On the X side, 12 other infrared beams were positioned 5 cm above the floor at 3-cm intervals, and the total number of beam crossings was counted as rearing behaviour. After the session, stools left on the floor were counted.

2.2.2. Acoustic startle reflex and prepulse inhibition test

Basic experimental settings were reported previously [42,53], we modified these for the present study. Briefly, the mouse was placed in a translucent acrylic cage (7 cm × 7 cm × 16.5 cm). Movements of the animal were detected by a piezoelectric accelerometer (GH313A, GA245SO; Keyence, Kyoto, Japan) attached at the bottom of cage. White noise at 115 dB (c) with duration of 50 ms was used as the acoustic startle stimulus (pulse). A noise prepulse of 85 dB (c)

was presented for 30 ms. Background noise was kept at a relatively constant level, 70–73 dB (c). The test session consisted of a total of 64 trials: 40 startle trials (habituation) without a prepulse, followed by 24 trials of prepulse test session. The mean inter-trial interval was 25 s (range, 15–45 s). In the prepulse trials prepulse with lead times of 50, 100, or 200 ms was followed by the pulse. In the prepulse test session, 12 pulse-alone trials and 12 prepulse trials were presented in random order. Relative startle response (RSR) was calculated using the formula RSR = PP/N, where PP designated the mean response with a prepulse, and N designated the mean response without a prepulse.

2.2.3. Water maze learning

A swimming tank 96 cm in diameter was used. Nontoxic India ink was added to the water to render it opaque. Water temperature was maintained at 20–24 °C. A platform 10 cm in diameter was positioned at a consistent point in the tank, submerged 5 mm below the surface of the water. In the learning trial, a mouse was placed in one of the three quadrants of the pool without platform. The experimenter determined the swimming time until reaching the platform (latency) using a stopwatch. When the animal reached the platform it was allowed to stay there for 10 s, and then was returned to a waiting box. If a mouse could not reach the platform within 60 s, the mouse was placed on the platform by the experimenter, and the latency was taken to be 60 s. The interval between trials was 30 s.

2.2.4. Passive avoidance learning

The apparatus consisted of two compartments, one lit and one dark, separated by a vertically sliding door. Mice initially were placed in the lit compartment. After the door was opened and the animal entered the dark compartment, the door was closed. After 10 s, a 3-s, 0.6-mA shock was delivered. The mouse was allowed to recover for 10 s and then returned to the home cage. Twenty-four hours later the mouse again was placed in the lit section with the door positioned opened to allow movement into the dark section. Latencies for stepping through the door were recorded.

2.2.5. Assessment of brain weight

After all behavioural tests, mice were killed by cervical dislocation. The brain was removed including the olfactory bulbs, the brainstem was cut at the level of the foramen magnum. Brain weighted at exactly 3 min after cervical dislocation.

2.3. Experiment 2: neuroanatomy

The effect of environmental manipulations on generation of neurons was examined using new mice.

2.3.1. Subjects

Twenty-eight male C57BL/6 mice, purchased from Nihon SLC (Shizuoka, Japan) when 3 weeks old, were reared for 8 weeks in four groups (each $n = 7$) with different housing conditions in the same manner as Experiment 1. Tap water and food (MF chow, Oriental, Tokyo, Japan) were continuously available.

2.4. Experimental protocol

2.4.1. Cell proliferation analysis

For assessment of cell proliferation *in vivo*, 5-bromo-2′-deoxyuridine (BrdU 200 mg/kg, Sigma–Aldrich) was administered intraperitoneally when mice reached to 12 weeks of age. After 24 h the four groups of mice were anaesthetized deeply with pentobarbital sodium (50 mg/kg) and fixed by transcardial perfusion with 4% paraformaldehyde. Then the brain was removed and postfixed for 24 h by immersion in 4% paraformaldehyde. Eight coronal slices 1 mm in thickness were made from the fixed forebrain using a rodent brain slicer (Acrylic Matrices, Alto, USA). Serial sections 20 μm in thickness were prepared from each slice with a vibratome (Leica, Wetzlar, Germany). Sections were subjected to double-labeling fluorescence immunohistochemistry with antibody to polysialylated neuronal cell adhesion molecule (PSA-NCAM, Chemicon International) as a marker of migrating neuronal progenitor cells (NPCs), and an antibody to BrdU (Boehringer Ingelheim, Mannheim, Germany).

Cells staining for both BrdU and PSA-NCAM according to confocal microscopy (Olympus, Tokyo Japan) were counted per high-power field (40× objective lens) as newly generated/proliferating neurons. For quantitative analysis, sections including the dentate gyrus of the hippocampus were stained, and BrdU/PSA-NCAM-positive cells in this granule cell layer were counted by two investigators blinded to the experimental protocol. The cell counted then was expressed as cells per millimetre of dentate gyrus. Cells in cerebral cortex stained for both BrdU and PSA-NCAM were counted in 10 fields of cingulate cortex, and the number of positive neocortical cells was expressed as cells per square millimetre.

3. Results

3.1. Behavioural data

3.1.1. Body weight change

Fig. 1 shows body weight change in the four groups of mice during the 8-week housing period. Mixed-type ANOVA indicated no significant main effect of group (G) [$F(3, 40) = 1.486$], while main effect of week (W) and interaction between G and W were significant [$F(7, 280) = 658.43$, $p < .0001$ and $F(21, 280) = 4.746$, $p < .0001$, respectively].

3.1.2. Open-field activity

Fig. 2 shows open-field performance and number of stools after 20 min. Fig. 2A indicates animal locomotion per 1-min block measured by mean number of beam crossing when two beams in each direction were positioned in 10-cm apart. The first 10 min was conducted in light, with the next 10 min in darkness. In general, crossing decreased as time passed during both lighting conditions. Mixed-type ANOVA including one between (group G) and two within-subject factors [light versus dark period (LD), and time in the session (T)] indicated that the main effect of T was significant [$F(9, 360) = 13.865$, $p < .0001$]. Interaction effects of T × G and LD × T were significant [$F(27, 360) = 1.949$, $p = .0037$ and $F(9, 360) = 7.517$, $p < .0001$, respectively]. However, main effects of G and LD and other interaction effects were not significant.

Fig. 2B presents mean number of rearing responses by 1-min block, measured as mean number of horizontal interruptions at 5 cm above the box floor. Mixed-type ANOVA showed that main effects of G, LD, and T all were significant [$F(3, 40) = 3.876$,

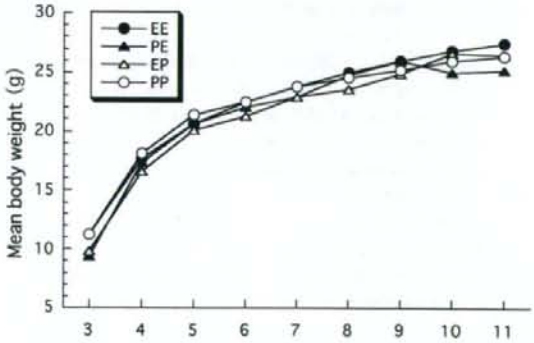

Fig. 1. Mean body weight change of four different housing groups from 3 to 11 weeks of age. Water and food were always available.

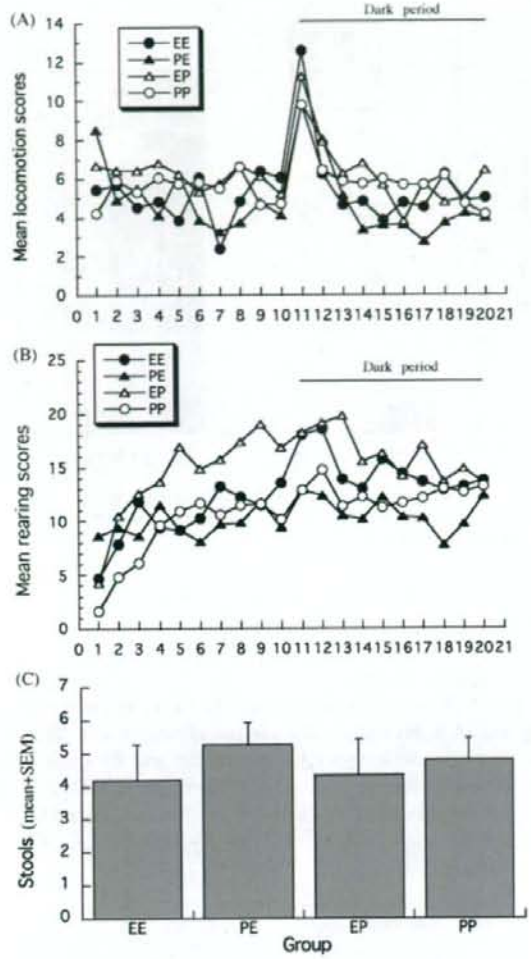

Fig. 2. Results of open-field test. Locomotion (A) counted by horizontal beam-cutting and rearing (B) measured by vertical beam-cutting were plotted. Ten minutes of light period were followed by 10 min of darkness, continuously. Stools found at the end of the session also were counted (C). All data are mean.

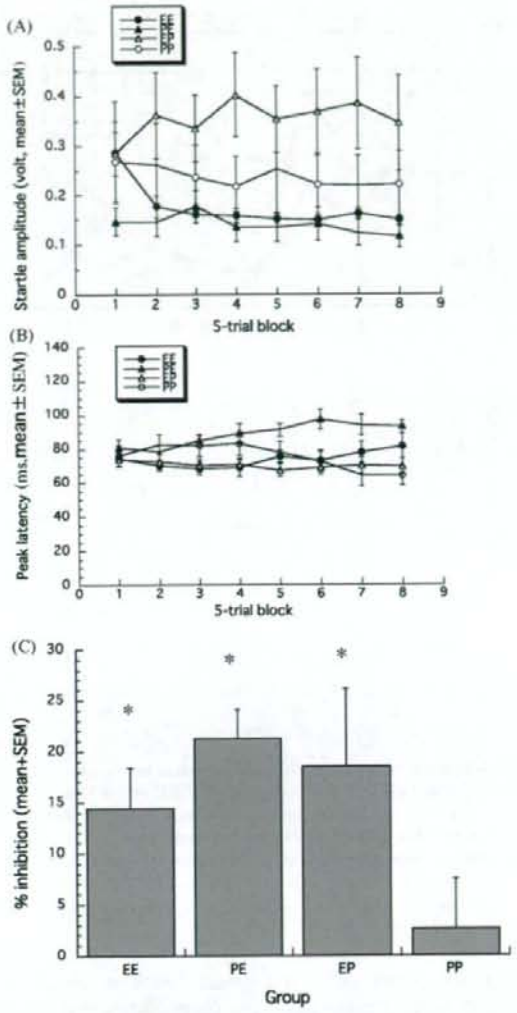

Fig. 3. Results for acoustic startle reflex and prepulse inhibition tests. Startle amplitude in volts (A), and peak latency during 40 trials of habituation (B) were plotted by 5-trial block, and prepulse inhibition by auditory prepulse with 50 ms of lead time (prepulse-pulse interval) condition (C) are shown. Asterisk shows significant inhibition. Data are mean ± SEM.

$p = .0159$; $F(1, 40) = 47.981$, $p < .0001$; $F(9, 360) = 3.682$, $p = .0002$, respectively]. Interaction effects of LD × G, T × G, LD × T, and LD × T × G were significant [$F(3, 40) = 2.937$, $p = .0448$; $F(27, 360) = 1.537$, $p = .0448$; $F(9, 360) = 17.048$, $p < .0001$; $F(27, 360) = 1.803$, $p = .0094$, respectively]. The group differences between EE and EP, EE and PE, EP and PE, and EP and PP were significant by the post hoc test.

Fig. 2C shows the mean number of stools per 20-min session. No group differences were observed [$F(3, 40) < 1$].

3.1.3. Startle reflex and prepulse inhibition

Fig. 3A shows mean amplitude of the auditory startle reflex in the 40 trials of the habituation period by 5-trial block. The results of mixed-type ANOVA indicated no main effects and the interaction effect were significant. Fig. 3B indicates mean peak latencies of the auditory startle reflex. Time to maximum movement amplitude in milliseconds after the start of the startle stimulus was recorded. Group EP showed shorter latency and group PE showed longer latency than the other groups. The results of the mixed-type ANOVA indicated that main effect of G and trial block (TB) [$F(3, 40) = 3.806$, $p = .0172$ and $F(7, 280) = 2.43$, $p = .0197$, respectively] and interactions of TB × G was significant [$F(21, 280) = 1.655$, $p = .0376$]. Fig. 3C shows mean percentage of prepulse inhibition under the auditory prepulse condition at a lead time of 50 ms, in which greatest inhibition was observed. Prepulse inhibition was smallest in the PP group, and inhibitions of the EE, PE and EP groups were significant ($Z = 3.48$, 2.43, and 6.92, respectively), but inhibition of PP mice was not ($Z = 0.53$).

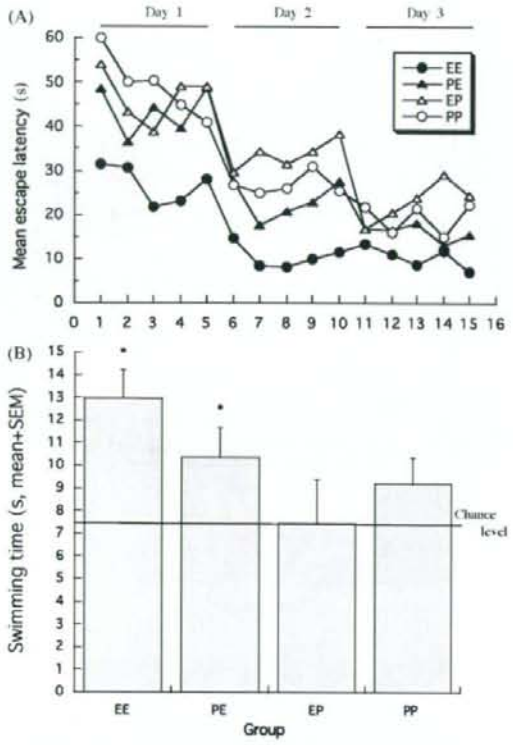

Fig. 4. Results for Morris water-maze learning. Mean latency of all trials in the three daily 5-trial sessions was plotted (A). The differences between EE and the other 3 groups, between PE and EP groups were significant. The results of probe test (B). Mice were allowed to search platform for 30 s. The mean of the total swimming time in the quadrant in which ever had contained the platform during training is shown. Asterisk shows significantly longer swimming time than chance level (7.5 s).

3.1.4. Water-maze learning

Fig. 4A shows mean water-maze latencies for all trials during three daily training sessions. From the first trial, EE mice performed better than other groups, reaching a plateau on the second training day. PP animals performed worst. The PE group showed learning curve intermediate between EE and PP groups. Results of mixed-type ANOVA including one between-subject factor (G) and two within-subject factors (day, D; trial, T) for water-maze learning showed that main effect of G and D were significant [$F(3, 40) = 7.637$, $p = .0004$ and $F(2, 80) = 65.883$, $p < .0001$, respectively]. Main effects of T [$F(4, 160) = 1.764$] and other interaction effects were not significant. The results of post hoc tests indicated group differences between EE and EP, EE and PE, EE and PP, and EP and PE were significant. Fig. 4B shows mean swimming time during 30 s probe test in the quadrant where the platform was placed during water-maze learning. Groups EE and PE showed significantly longer swimming time than the chance level (7.5 s) [$Z = 4.409$, $p < .01$ and $Z = 2.875$, $p < .01$, respectively], but the swimming time of groups PP and EP were not significantly different from the chance level [$Z = .03$ and 1.496, respectively]. Groups EE and PE were better at maze learning than the other two groups,

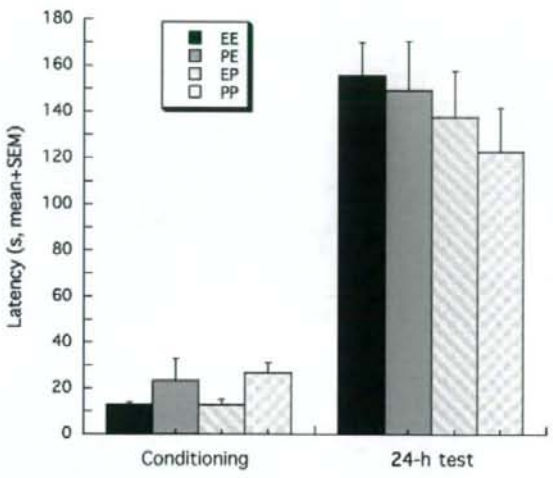

Fig. 5. The results of passive avoidance test. Step-through latencies from light to dark compartments in the conditioning trial (left) and the 24-h test trial (right) are plotted (mean + S.E.M.).

and memorized relatively well where the platform had been placed.

3.1.5. Passive avoidance

Fig. 5 shows mean step-through latencies in the conditioning and 24-h test trials of the passive avoidance test. Although PP mice showed longer latency than EE and EP groups during the conditioning trial, ANOVA performed including the respective trials indicated no group differences for conditioning or 24-h test trials [$F(3, 40) = 2.599$, $p = .065$ and $F(3, 40) < 1$, respectively].

3.2. Neuroanatomic data

3.2.1. Brain weight

Environmental change affected brain weight as well as behaviour. Fig. 6 shows mean weight of the brain determined after completion of all behavioural tests. Animals were 13 weeks old. EE and PE mice had heavier brains than PP and EP animals. ANOVA showed this group effect to be significant [$F(3, 34) = 3.288$, $p < .0323$]. Results of the group comparisons by post hoc tests indicated that group differences between EE and EP, EP and PE, and PE and PP were significant.

3.2.2. Induction of neuronal regeneration in situ

To examine the basis for increased brain weight in the enriched condition, generation of neuronal cells in cerebral cortex and hippocampus was assessed by *in vivo* BrdU labeling. Sections were visualised by confocal microscopy with antibody labeling for BrdU and PSA-NCAM. Cellular profiles for both markers were considered newly generated neurons (Fig. 7). Neuronal generation continued during the enriched condition, but decreased after 2 weeks in the impoverished condition. Newly generated neurons were present at a constant but low level in continuously impoverished (PP) mice.